Available online at www.sciencedirect.com
ScienceDirect
Journal of Sound and Vibration 313 (2008) 510–524
JOURNAL OF SOUND AND VIBRATION
www.elsevier.com/locate/jsvi

Analysis of absorption and reflection mechanisms in a three-dimensional plate silencer

Chunqi Wang[a,*], Lixi Huang[b]

[a]*Department of Mechanical Engineering, The Hong Kong Polytechnic University, Kowloon, Hong Kong*
[b]*Department of Mechanical Engineering, The University of Hong Kong, Pokfulam Road, Hong Kong*

Received 22 April 2007; received in revised form 13 November 2007; accepted 17 December 2007
Available online 6 February 2008

Abstract

When a segment of a rigid duct is replaced by a plate backed by a hard-walled cavity, grazing incident sound waves induce plate vibration, hence sound reflection. Based on this mechanism, a broadband plate silencer, which works effectively from low-to-medium frequencies have been developed recently. A typical plate silencer consists of an expansion chamber with two side-branch cavities covered by light but extremely stiff plates. Such a configuration is two-dimensional in nature. In this paper, numerical study is extended to three-dimensional configurations to investigate the potential improvement in sound reflection. Finite element simulation shows that the three-dimensional configurations perform better than the corresponding two-dimensional design, especially in the relatively high frequency region. Further analysis shows that the three-dimensional design gives better plate response at higher axial modes than the simple two-dimensional design. Sound absorption mechanism is also introduced to the plate silencer by adding two dissipative chambers on the two lateral sides of a two-cavity wave reflector, hence a hybrid silencer. Numerical simulation shows that the proposed hybrid silencer is able to achieve a good moderate bandwidth with much reduced total length in comparison with pure absorption design.

1. Introduction

Previous studies have shown that, in a duct, a tensioned membrane or a simply supported plate covering a side-branch rigid cavity can function effectively as a wave reflector over a broad range of low-to-medium frequencies [1,2]. Such a device can be named either a drumlike silencer or a plate silencer depending on whether a tensioned membrane or plate is used to reflect the incident sound wave. The prototype drumlike silencer has been tested successfully for the conditions of without and with flow [3,4]. Note that plates and membranes have also been used in many other noise abatement applications. For example, panel absorbers were used in broadcasting studios [5–7] and other architectural practices, and membrane absorbers were used as a splitter silencer in the form of arrays of Helmholtz resonators [8]. In all these applications, the panel, or membrane, is a component of resonator, which works for a relatively narrow frequency band for one such

*Corresponding author. Tel.: +852 2766 4247; fax: +852 2365 4703.
E-mail address: chunqiwang@yahoo.com.cn (C. Wang).

0022-460X/$ - see front matter © 2007 Elsevier Ltd. All rights reserved.
doi:10.1016/j.jsv.2007.12.027

resonator, and the structural mass is a means to achieve a low resonance frequency. For the drumlike or plate silencer, the most desirable properties of the membrane/plate are the high stiffness and low mass density, which contrasts with the characteristics of the use of panels elsewhere [5–8]. The main difference between the drumlike/plate silencer and the previous use of membrane or panel in resonators is that the former aims for a broadband performance with one set of membrane or plate.

Besides the broad stopband in low-frequency region, the plate silencer shares another advantage of creating zero back pressure. It is well known that a well-designed expansion chamber-type muffler (for example, the vehicle exhaust muffler) can also treat the low-frequency noise effectively. However, the most important detrimental effect in a vehicle muffler design is the back pressure (pressure loss) due to the discontinuity of the duct cross-section. The back pressure results in extra power consumption. As a result, more noise could be generated by the additional power required to overcome the pressure loss. To reduce the back pressure, straight-through concentric resonator, plug muffler, and three-duct cross-flow muffler have been proposed and their performance has been experimentally verified [9]. These designs can reduce but cannot eliminate the back pressure. In the design of the plate silencer, the plate is flush mounted with the duct wall and there is no sudden change of the duct area. Thus, the flow can pass the silencer smoothly without causing any extra pressure loss when compared with a uniform duct of the same total length.

In all previous studies on drumlike/plate silencers, two rigid cavities are equipped on two opposite sides of a rectangular duct [1–4]. The plates, which are flush mounted with the duct walls, cover the cavities completely. Such a configuration is in fact two-dimensional (2D), say on x–y plane. In this study, numerical study is extended to three-dimensional (3D) designs to investigate the potential improvement in sound reflection by adopting better geometrical configurations. Also, the extension to 3D design will feed the needs of various practical applications where a 3D configuration is more appropriate (for example, circular ducts). Four different 3D configurations are investigated and compared with the 2D design. One direct way to construct a 3D plate silencer is to combine two identical two-cavity plate silencers, one on x–y plane and the other on x–z plane, in parallel to form a so-called "four-cavity plate silencer", in which all of the four sides of the rectangular duct are covered by plates. The cross-section of such silencer is shown in Fig. 3(a). Alternatively, the four cavities can be replaced by a circular chamber and the rectangular duct itself may also be replaced by a quasi-circular one. Unlike the 2D plate silencer studied before, both the four-cavity and the circular designs involve many 3D effects, such as the loading on one plate caused by the vibration of neighboring plates, as well as the effect of the 3D cavity. The method of solution developed for the 2D system in Ref. [1] may be extended to analyze the current problem, but a finite element method (FEM) is more convenient to model and simulate such a coupled 3D system.

The second type of 3D silencer investigated here is a hybrid silencer combining reactive and dissipative elements in a parallel manner. The motivations for such design are as follows. Like any other reactive silencers, the plate silencer generally has poor performance at high frequencies. On the other hand, dissipative silencers, which often are filled with sound absorbing materials such as fiberglass, can attenuate the high-frequency noise easily. But their performance (attenuation) is rather poor at low frequencies. Hence, it is expected that a combination of a reactive plate silencers with the dissipative elements can lead to a silencer effective from low-to-high-frequency range. Additionally, the interaction between plate vibration and sound dissipation may improve the silencing performance at low frequencies, which is also a desirable property for the low-frequency wave reflector itself. One straightforward design of a hybrid silencer is to add sound-absorbing materials to the cavity covered by the vibrating plate, as investigated in Ref. [2]. Numerical results showed that the use of sound absorbing material in the covered cavity is marginally beneficial for the stop bandwidth since the presence of the sound absorbing material in the cavity has the general effect of suppressing the plate response leading to reduced wave reflection capability. Instead of filling the cavity covered by plate with sound absorbing material, the alternative method is to fill neighboring cavities reserved for this purpose in a 3D design. For example, in a four-cavity design similar to the cross-section view shown in Fig. 3(a), a pair of two opposing cavities are used for plate silencer, while the other two are filled with sound absorbing material. The result is called a hybrid silencer arranged in parallel occupying a small axial distance. On the other hand, when four plate-covered cavities are all used for sound reflection, it is designated as a four-cavity wave reflector.

In what follows, finite element simulation shows that the silencing performance of the 3D wave reflectors is extended into both lower and higher frequencies compared with its 2D counterpart of the same total cavity volume. For the hybrid silencer, it is found that such a combination of sound absorption and reflection mechanisms is able to achieve a moderate bandwidth with a much reduced total axial length.

2. Theoretical outline

2.1. Finite element modeling

The finite element modeling procedure for a four-cavity wave reflector is presented. For other 3D plate silencers considered in this study, similar procedures could be followed, hence the details are not given here. The so-called four-cavity wave reflector can be considered as a parallel combination of two two-cavity plate silencers, in which each module of cavity-backed plate is assumed to be identical to the opposite one. The cross-section of the rigid duct is assumed to be square and the height is h. Only one quarter of the four-cavity wave reflector is modeled because of the symmetry in the system. As shown in Fig. 1, the bottom cavity of depth h_{c1} is covered by a plate (a–b–c–d) of length L and width h, or half-width $h/2$ in the quarter model in Fig. 1. Similarly, the back cavity of depth h_{c2} is covered by a plate (b–e–f–c) of the same size as the plate (a–b–c–d). The leading and trailing edges of the plates, that is, a–b, c–d, b–e, and c–f are simply supported. These edges may also be clamped as in the 2D study reported earlier [10], and similar results can be obtained and are not presented here. The other four edges are set free to allow the plate to respond to incident sound waves with high vibration magnitude. Suppose that a plane incident sound wave comes from the left to the right with unit amplitude

$$p_i = \mathrm{e}^{\mathrm{i}(\omega t - k_0 x)} \tag{1}$$

and it induces the plates (a–b–c–d) and (b–e–f–c) to vibrate with normal displacement of complex amplitude $\eta_1(x, y)$, $\eta_2(x, z)$ with the same time dependence, $\exp(\mathrm{i}\omega t)$, which is henceforth omitted. The plate motion radiates sound in both direction of the duct axis, $\pm x$, and imposes a radiation pressure on the plate surface. The problems of acoustics and plate vibration are coupled strongly.

Femlab® is a software package for solving partial differential equations based on FEM. Because of its strong multiphysics capability, Femlab® is chosen to solve the current vibroacoustic coupling problem. The code will be validated by comparing its result for a different configuration for which semi-analytical method has been established. In the current numerical simulation, there are two types of physical domains. One is the 3D acoustic domain for the fluid (air) in the duct, the bottom and back cavities. The other is the 2D domain for the plates, which is modeled based on the Mindlin plate theory. The duct and cavities are modeled by

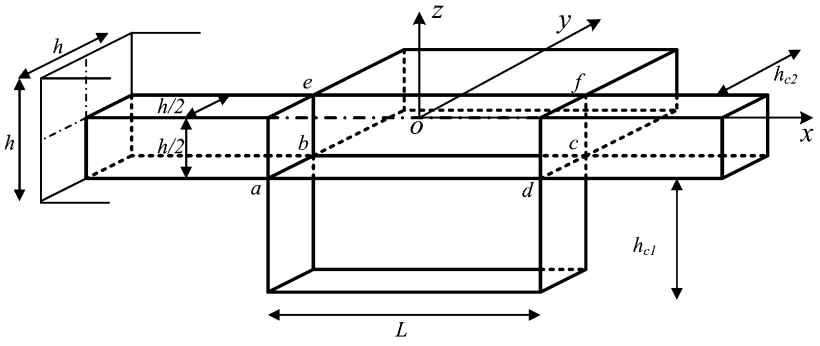

Fig. 1. The quarter model of a four-cavity wave reflector (or hybrid silencer). The bottom and top (not shown) cavities have a length of L and depth h_{c1}; the back and front (not shown) cavities have a length of L and depth h_{c2}. In the case of a hybrid silencer, the bottom and top cavities are used to reflect sound and the other two cavities are filled with sound absorbing materials. Otherwise, all of the four cavities are for sound reflection.

Helmholtz equation using velocity potential ϕ,

$$\left(\nabla^2 - \frac{1}{c_0^2}\frac{\partial^2}{\partial t^2}\right)\phi = 0. \tag{2}$$

The velocity potential ϕ is related to sound pressure p and acoustic particle velocity u as

$$p = -\rho_0 \frac{\partial \phi}{\partial t}, \quad u = \nabla\phi, \tag{3}$$

where c_0 is the speed of sound in air, and ρ_0 is the density of air. The vibroacoustic coupling between the duct, the plate (a–b–c–d) and the bottom cavity is modeled as below. The vibration of plate (a–b–c–d) is governed by the following equation:

$$m_1 \frac{\partial^2 \eta_1}{\partial t^2} + B_1 \nabla^4 \eta_1 + \Delta p = 0, \tag{4}$$

where B_1 is the bending stiffness of the plate, m_1 is the plate mass per unit area, and Δp is the sound pressure difference across the interface at $z = -h/2$,

$$\Delta p = p|_{z=(-h/2)+} - p|_{z=(-h/2)-}. \tag{5}$$

Meanwhile, the motion of the plate is also coupled to the sound wave in the duct and bottom cavity by a kinematic condition on both sides of the plate

$$\frac{\partial \eta_1}{\partial t} = \left.\frac{\partial \phi}{\partial z}\right|_{z=(-h/2)+} = \left.\frac{\partial \phi}{\partial z}\right|_{z=(-h/2)-}. \tag{6}$$

Eqs. (4)–(6) describe the vibroacoustic interaction between the plate (a–b–c–d), the duct, and the bottom cavity completely. The vibroacoustic coupling between the plate (b–e–f–c), the duct, and the back cavity can be treated in the same way. For frequencies below the first cut-on frequency of the duct, the inlet and exit boundaries are governed by simple traveling wave relationships:

$$\phi_\pm = A_\pm \exp(\mathrm{i}\omega t \mp \mathrm{i}k_0 x), \quad p_\pm = \pm\rho_0 c_0 u, \tag{7}$$

where the two signs of $\pm$ apply to the right-going and left-going waves, respectively. At the exit, an anechoic boundary condition is assumed so that $p = \rho_0 c_0 u$ or

$$\frac{\partial \phi}{\partial x} + \mathrm{i}k_0 \phi = 0. \tag{8}$$

At the inlet, the incident sound wave p_i is mixed with the unknown reflected sound wave p_r. Noting that the reflected sound wave p_r is a simple left-going plane wave, the total sound pressure wave p, the total acoustic particle velocity u, the incident sound wave p_i, the incident acoustic particle velocity u_+, the reflected sound wave p_r and the reflected acoustic particle velocity u_- satisfy the following relationships:

$$p_r = p - p_i, \quad u_- = u - u_+, \quad p_r = -\rho_0 c_0 u_-. \tag{9}$$

Thus,

$$p - p_i = -\rho_0 c_0 (u - u_+), \tag{10}$$

$$p + \rho_0 c_0 u = 2p_i \tag{11}$$

and the boundary condition at the inlet is given as, assuming $p_i = 1$,

$$\frac{\partial \phi}{\partial x} - \mathrm{i}k_0 \phi = \frac{2}{\rho_0 c_0}. \tag{12}$$

The walls of the duct and cavities are assumed to be acoustically rigid, so the particle velocity normal to the wall vanishes. The boundary condition on the wall is then

$$\frac{\partial \phi}{\partial n} = 0, \tag{13}$$

where n is the outward normal direction. Eqs. (2)–(13) are solved in Femlab® with the plate surface velocity and pressure coupled across the structural and fluid domains, and the transmission loss (TL) of the plate silencer is found as

$$\mathrm{TL} = 10\log_{10}\left(\frac{\int_{\mathrm{exit}} |\phi|^2 \,\mathrm{d}s}{\int_{\mathrm{inlet}} |\phi_i|^2 \,\mathrm{d}s}\right), \tag{14}$$

where ϕ_i is the velocity potential of the incident sound wave, and "inlet" and "exit" refer to the inlet and exit cross-section, respectively. The energy coefficients of sound wave absorption (if applicable), α, and reflection, β, are evaluated as

$$\alpha = 1 - \frac{\int_{\mathrm{inlet}} |\phi - \phi_i|^2 \,\mathrm{d}s + \int_{\mathrm{exit}} |\phi|^2 \,\mathrm{d}s}{\int_{\mathrm{inlet}} |\phi_i|^2 \,\mathrm{d}s}, \tag{15}$$

$$\beta = \frac{\int_{\mathrm{inlet}} |\phi - \phi_i|^2 \,\mathrm{d}s}{\int_{\mathrm{inlet}} |\phi_i|^2 \,\mathrm{d}s}. \tag{16}$$

The hybrid silencer is constructed by adding two dissipative chambers on the two lateral sides of a two-cavity wave reflector. So, the outlook of such a configuration resembles that of a four-cavity wave reflector, and the configuration of the quarter model in Fig. 1 can also be used to describe the hybrid silencer. Suppose the back cavity is the dissipative chamber, and the bottom cavity is covered by plate and is employed to reflect the incident sound. The governing equations of the sound in the duct and the bottom cavity, as well as the boundary conditions imposed on the inlet, the exit, the cavity and duct walls, and the plates are the same as those for the four-cavity wave reflector. For the dissipative chamber (the back cavity), the sound absorbing material is treated as an equivalent fluid with complex density and speed of sound. Following Mechel and Vér [11], the wave equation in the sound absorbing material may be established by combining the mass and momentum conservation laws. Similar to sound wave propagation in lossless fluid, a velocity potential can be introduced and is related to sound pressure and velocity perturbations as follows:

$$u = \nabla\phi, \quad p = -\rho_c \frac{\partial\phi}{\partial t}, \quad \left(\nabla^2 - \frac{1}{c_c^2}\frac{\partial^2}{\partial t^2}\right)\phi = 0, \tag{17}$$

where ρ_c, u, and c_c are, respectively, the complex density, particle velocity and complex speed of sound. The complex density ρ_c and speed of sound c_c are given by empirical formulas using the data of glass fiber [11]

$$\begin{aligned}
E &= \rho_0 f / R_{\mathrm{sam}},\\
\frac{c_0}{c_c} &= 0.396E^{-0.458} + \mathrm{i}\left(1 + 0.135E^{-0.646}\right) \quad (E \leqslant 0.025),\\
\frac{\rho_c c_c}{\rho_0 c_0} &= \left(1 + 0.0668E^{-0.707}\right) - \mathrm{i} \times 0.196E^{-0.549} \quad (E \leqslant 0.025),\\
\frac{c_0}{c_c} &= 0.179E^{-0.674} + \mathrm{i}\left(1 + 0.102E^{-0.705}\right) \quad (E > 0.025),\\
\frac{\rho_c c_c}{\rho_0 c_0} &= \left(1 + 0.0235E^{-0.887}\right) - \mathrm{i} \times 0.0875E^{-0.707} \quad (E > 0.025),
\end{aligned} \tag{18}$$

where R_{sam} is the flow resistance of the sound absorbing material.

For convenience, parameters are normalized by three basic quantities: air density ρ_0, speed of sound c_0, and the duct height h. For example, time and pressure quantities are normalized by h/c_0 and $\rho_0 c_0^2$, respectively. The normalization scheme for the four most important parameters: frequency, plate-to-air mass ratio, bending stiffness, and flow resistance are given below:

$$f^* = \frac{fh}{c_0}, \quad m^* = \frac{m_s}{\rho_0 h}, \quad B^* = \frac{B}{\rho_0 c_0^2 h^3}, \quad R^*_{\mathrm{sam}} = \frac{R_{\mathrm{sam}} h}{\rho_0 c_0}. \tag{19}$$

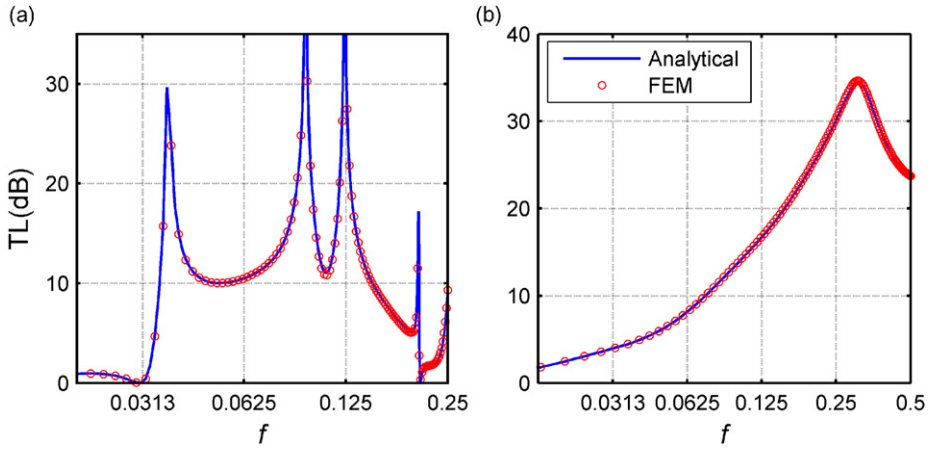

Fig. 2. Comparison between the FEM calculation (open circles) and the semi-analytical solution (solid lines): (a) TL spectra of a two-cavity wave reflector. The cavities have a length of $L = 5$ and depth $h_c = 1$. The plates with stiffness $B = 0.129$ and mass ratio $m = 1$ are simply supported at the leading and trailing edges. (b) TL spectra of duct lining (flow resistance $R_{\text{sam}} = 1.4$) filling two cavities of depth $h_c = 1$ and length $L = 5$.

For simplicity, the asterisk is omitted for the dimensionless parameter in the following presentation. Thus defined, the dimensionless frequency of $f = 0.5$ is the first cut-on frequency of the square duct of cross-section h by h. To avoid confusion, the physical unit will be given whenever a dimensional quantity is used.

2.2. Model validation

The accuracy of the finite element simulation depends mostly on the mesh model and the solver. To ensure that the prediction is reliable, it is necessary to verify the finite element analysis against a well-established method suitable for a simpler configuration. By assuming the duct wall facing plate (*b–e–f–c*) or plate (*a–b–c–d*) to be acoustically solid, the hybrid silencer becomes a separate plate silencer or dissipative chamber accordingly. Fig. 2(a) compares the TL spectrum of the plate silencer simulated by the FEM model with that from the semi-analytical solution following the usual Galerkin procedure of modal expansion [2]. The cavity geometry is of $L = 5h$, $h_{c1} = h$ and the properties of the plate (*a–b–c–d*) are $B_1 = 0.129$ and $m_1 = 1$. The leading and trailing edges of the plate are simply supported. Fig. 2(b) compares the simulated spectrum of duct lining filling two cavities of depth $h_{c2} = h$ and $L = 5h$ with that from the semi-analytical solution [12]. The dimensionless flow resistance is $R_{\text{sam}} = 1.4$. The semi-analytical solutions are shown in solid lines, and the FEM simulations are given as open circles. In the FEM simulation, a total of 1792 Lagrangian, hexahedral elements are used for the acoustic domain and 380 Lagrangian, triangular elements are employed for the 2D plate, while the number of axial plate modes in the semi-analytical method is 25. As shown in Fig. 2(a) and (b), the FEM simulation matches with the semi-analytical results very well, and no visible deviation between the results from the two methods can be observed except at the resonant peaks in Fig. 2(a). In the design of the plate silencer, the main concern is the stopband in which the TL is above a criterion value TL_{cr} over the whole frequency band, and the absolute values at the resonant peaks are of little concern. In light of this, this finite element simulation is regarded as sufficiently accurate for the purpose of this study.

3. 3D wave reflector

A comparative study is conducted between the 3D and 2D wave reflectors to examine the potential performance improvement by adopting the 3D configuration. To facilitate the comparison, the plate-to-air mass ratio and the total cavity volume are kept equal for all the wave reflectors studied.

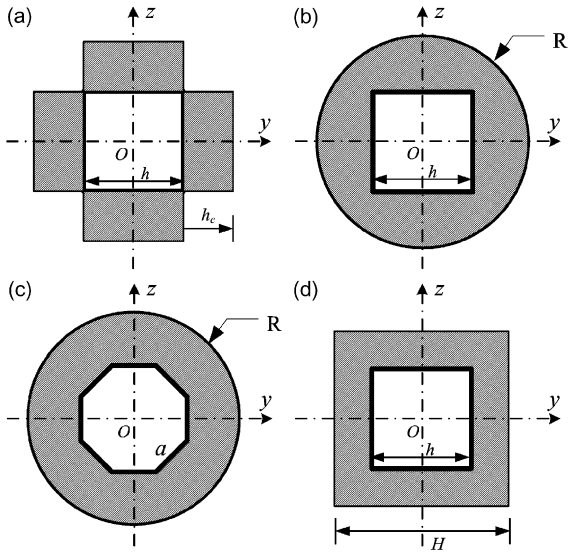

Fig. 3. Cross-sections for the 3D wave reflectors: (a) Four-cavity wave reflector. Four backing cavities with depth h_c are shown in shadowed area. Four plates forming part of the otherwise rigid duct walls are shown in thick solid lines. (b) Rectangular duct with circular chamber of radius R. (c) Regular octagon duct with circular chamber of radius R. The side length of the octagon a satisfies the relationship $2(1+\sqrt{2})a^2 = h^2$. (d) Rectangular duct with rectangular chamber. The side lengths for the outer and inner square cross-sections are H and h, respectively.

3.1. Performance of 3D wave reflectors

Fig. 3(a)–(d) shows the cross-sections of four types of 3D wave reflectors, which are designated as plate silencer I, II, III, and IV in the following text, respectively. Plate silencer I is a four-cavity wave reflector and a quarter model for such a configuration has already been given in Fig. 1. The four backing cavities are indicated by shadowed area in Fig. 3(a). For plate silencer II shown in Fig. 3(b), the four backing cavities are replaced by a circular chamber of radius R, which is also shown in shadowed area. Plate silencer III shown in Fig. 3(c) is constructed by a regular octagon duct of side length a with a circular backing chamber of radius R. The last one shown in Fig. 3(d) is a square duct with a square chamber put outside. For plate silencers I, II, and IV, four plates of width h are flush mounted with the duct walls, while for plate silencer III, eight plates of width a are required.

The silencing performance of the wave reflectors is affected by several variables related to the backing cavity and plate properties. To simplify the investigation, the following parameters are set as default values for all the four 3D plate silencers:

$$m = 1, \quad L = 5, \quad \Lambda = 10, \tag{20}$$

where m is the plate-to-air mass ratio, L is the cavity (or plate) length, and Λ is the total cavity volume, that is, the total added volume occupied by the backing cavities. For instance, assuming the shadowed area in Fig. 3(a) is S, the total cavity volume Λ of plate silencer I is then defined as

$$\Lambda = SL. \tag{21}$$

The selection for the above default configuration in Eq. (20) is to facilitate the comparison between the 2D plate silencer studied in Huang [2] and the 3D plate silencers in the current study. In the previous theoretical study conducted [2], an optimal cavity shape with $L = 5$ and $h_c = 1$ was chosen to investigate the two-cavity plate silencer. So, a total cavity volume $\Lambda = 10$ for the 3D configurations guarantees that the expansion ratios for both the 2D and 3D configurations are the same. The stopband of the plate silencer is defined as a continuous frequency band, $f \in [f_1, f_2]$, in which the TL is above a criterion value $\mathrm{TL_{cr}}$. The silencing performance of the 3D plate silencers is optimized. With the default parameters specified in Eq. (20), the

so-called optimization is performed by varying the bending stiffness gradually and searching for the optimal bending stiffness B_{opt} so that the ratio f_2/f_1 is the highest. Since special emphasis is put on the low-frequency noise, f_2/f_1 instead of (f_2-f_1) is chosen as the objective function to be maximized in the optimization exercise. The criterion value TL_{cr} is somewhat arbitrary but a procedure described in Huang [12] recommends that the value be chosen as the peak TL for an expansion chamber with the added volume is three times the actual added volume used by the plate silencer. For a total cavity volume of $\Lambda = 10$, this value can be calculated and rounded up to 10 dB.

3.1.1. Four-cavity wave reflector

Plate silencer I is a four-cavity wave reflector. The properties of the four cavities and plates are assumed to be identical, namely, $h_{c1} = h_{c2} = h_c$, $m_1 = m_2 = m$ and $B_1 = B_2 = B$. For a four-cavity wave reflector with cavity length L and cavity depth h_c, the total cavity volume is

$$\Lambda = 4Lh_c h, \tag{22}$$

where $h = 1$ is the duct height that can be omitted. Such a definition of total cavity volume is equivalent to that for the two-cavity plate silencer in [2]

$$\Lambda' = 2L'h'_c, \tag{23}$$

where L' and h'_c are the cavity length and depth for the two-cavity plate silencer. Hence, the two definitions are used equally without further notational distinctions. With $m = 1$, $\Lambda = 10$, and $L = 5$ given, the following set of optimal results is found for plate silencer I:

$$B_{opt} = 0.215, \quad f_1 = 0.0341, \quad f_2 = 0.211. \tag{24}$$

For the two-cavity configuration, the corresponding maximum stopband found in Ref. [2] is $f \in [0.0353, 0.149]$, with the logarithmic bandwidth $f_2/f_1 = 4.25$. Fig. 4 compares the TL spectra between the four- and two-cavity wave reflectors. As shown in Fig. 4, the performance improvement of the four-cavity configuration comes from both higher and lower frequencies, although the difference between the lower frequency limits of the two configurations is very small.

3.1.2. Rectangular duct with circular chamber

Plate silencer II is constructed by replacing the four rectangular cavities of the four-cavity wave reflector with a circular chamber of radius R. The four sides of the rectangular duct are still covered by four plates with leading and trailing edges simply supported. Similar to the four-cavity configuration, a quarter model for the circular design is established for the finite element simulation. The modeling procedure is almost the same as that for plate silencer I except that the four cavities are replaced by one circular chamber as shown in Fig. 3(b). The 3D mesh shown in Fig. 5 is generated by extruding the triangular mesh in one cross-section of the chamber along the x direction, and a total of 6780 prism (wedge) elements are created for the quarter model.

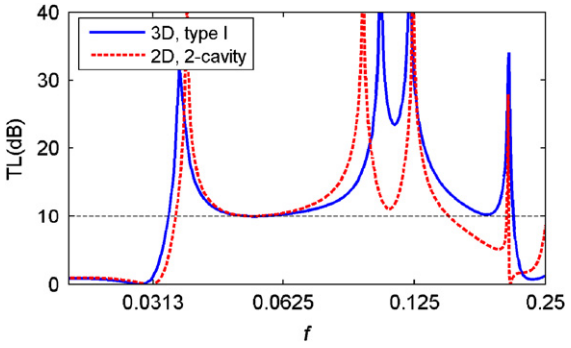

Fig. 4. TL comparison between the 3D plate silencer I (four-cavity, $B_{opt} = 0.215$) and the 2D design (2-cavity, $B_{opt} = 0.129$). The two configurations have the same cavity volume $\Lambda = 10$, cavity length $L = 5$, and mass ratio $m = 1$.

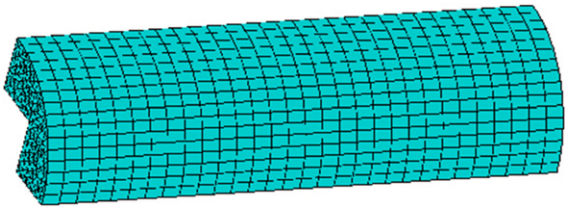

Fig. 5. Geometry and structured mesh for the circular chamber (quarter model).

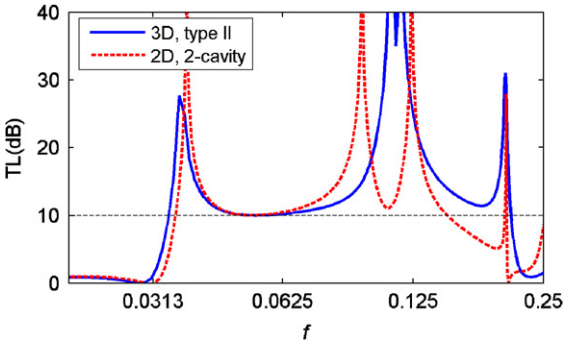

Fig. 6. TL comparison between the 3D plate silencer II (rectangular duct with circular chamber, $B_{\text{opt}} = 0.212$) and the 2D design (2-cavity, $B_{\text{opt}} = 0.129$). The two configurations have the same cavity volume $\Lambda = 10$, cavity length $L = 5$, and mass ratio $m = 1$.

With the cross-section of plate silencer II given in Fig. 3(b), the total cavity volume of the circular chamber is calculated as

$$\Lambda = (\pi R^2 - h^2)L, \tag{25}$$

where R and L are the radius and length of the circular chamber, and $h = 1$ is the height of the duct. For the default configuration specified in Eq. (20), the radius of the circular chamber can be found as $R = \sqrt{\pi/3}$, and the following optimal results are found for plate silencer II:

$$B_{\text{opt}} = 0.212, \quad f_1 = 0.0339, \quad f_2 = 0.21. \tag{26}$$

Fig. 6 shows the corresponding TL spectrum of plate silencer II (solid line), together with that for the two-cavity design for comparison. The optimal stopband for plate silencer II is $f \in [0.0339, 0.21]$ with $f_2/f_1 = 6.2$, which also compares favorably with the stopband $f \in [0.0353, 0.149]$ for the two-cavity design.

3.1.3. Regular octagon duct with circular chamber

Circular ducts are also widely used in industry. Plate silencer III shown in Fig. 3(c) approximates the circular duct using a regular octagon of side length a. Such a configuration can be simulated in the same way as that for a rectangular duct with circular chamber. The cross-section of the octagon duct has the same area A_{oct} as the rectangular duct for plate silencer I and II, that is,

$$A_{\text{oct}} = 2\left(1 + \sqrt{2}\right)a^2 = h^2, \tag{27}$$

where a is the side length of the regular octagon and $h = 1$ is the height of the rectangular duct. The radius of the circular chamber is also $R = \sqrt{\pi/3}$ so that the total cavity volume is kept at $\Lambda = 10$. Following the same optimization procedure, the widest stopband is found with the following set of parameters:

$$B_{\text{opt}} = 0.188, \quad f_1 = 0.0335, \quad f_2 = 0.212. \tag{28}$$

The corresponding TL spectrum is shown in Fig. 7 in solid line.

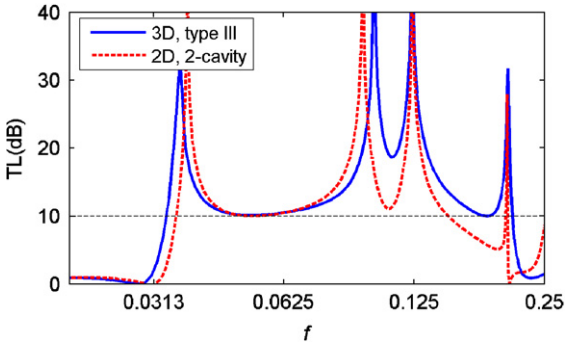

Fig. 7. TL comparison between the 3D plate silencer III (regular octagon duct with circular chamber, $B_{opt} = 0.188$) and the 2D design (2-cavity, $B_{opt} = 0.129$). The two configurations have the same cavity volume $\Lambda = 10$, cavity length $L = 5$, and mass ratio $m = 1$.

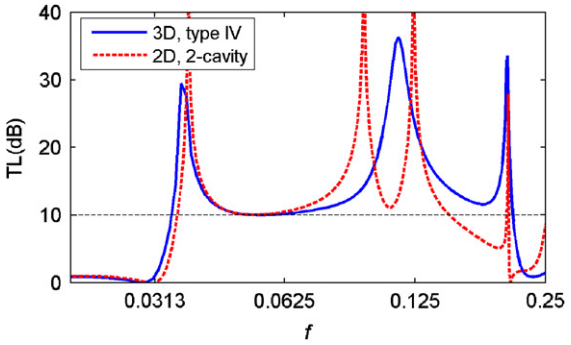

Fig. 8. TL comparison between the 3D plate silencer II (rectangular duct with rectangular chamber, $B_{opt} = 0.215$) and the 2D design (2-cavity, $B_{opt} = 0.129$). The two configurations have the same cavity volume $\Lambda = 10$, cavity length $L = 5$, and mass ratio $m = 1$.

3.1.4. Rectangular duct with rectangular chamber

For plate silencer IV, the four plates covering the square duct are backed by a rectangular chamber of cross-section $H \times H$, as shown in Fig. 3(d). In order to keep the same total cavity volume of the silencer installation, the side length of the outer rectangular chamber is specified as $H = \sqrt{3}h$. The performance for the plate silencer IV is optimized as

$$B_{opt} = 0.215, \quad f_1 = 0.0341, \quad f_2 = 0.211 \tag{29}$$

and the corresponding TL spectrum is shown in Fig. 8 in solid line. Unlike in the previous three cases studied, the second and third spectral peaks merge and only three peaks appear in the TL spectrum for plate silencer IV. Nevertheless, plate silencer IV can also achieve a similar wide stopband from 0.0341 to 0.211, as shown in Fig. 8.

So far, four types of 3D configurations have been simulated. Compared with the 2D design, the 3D configurations have two obvious benefits in common. First, the four 3D silencers have much wider stopbands than the 2D design of the same total cavity volume. Of the four 3D silencers studied, the design of a regular octagon duct with circular chamber (type III) has the highest bandwidth $f_2/f_1 = 6.33$, followed by the design of a rectangular duct with circular chamber (type II, $f_2/f_1 = 6.20$), the design of four-cavity wave reflector (type I, $f_2/f_1 = 6.19$), and the design of rectangular duct with rectangular chamber (type IV, $f_2/f_1 = 6.19$). Hence, all the four 3D silencers outperform their 2D counterpart, which having a maximum bandwidth of $f_2/f_1 = 4.25$ [2]. As shown in Figs. 4, 6–8, the 3D designs extend the stopband in both lower and higher frequency regions relative to the corresponding 2D design, although the performance improvement in the higher frequency region is more significant than that in the lower frequency region. Second, as the cavity volume is distributed uniformly around the four sides of the duct, the proposed 3D designs are more compact in terms of the

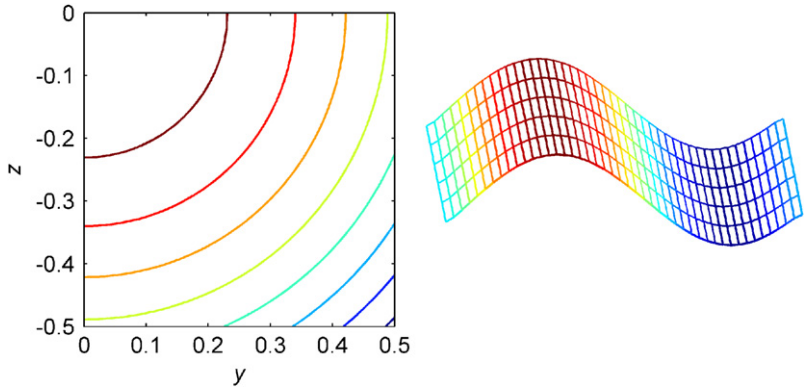

Fig. 9. Three-dimensional effect of the four-cavity wave reflector: (a) Contour of the velocity potential inside the duct at the cross-section of $x = 0$ for $f = 0.05$. (b) Velocity response of the plate at frequency $f = 0.05$.

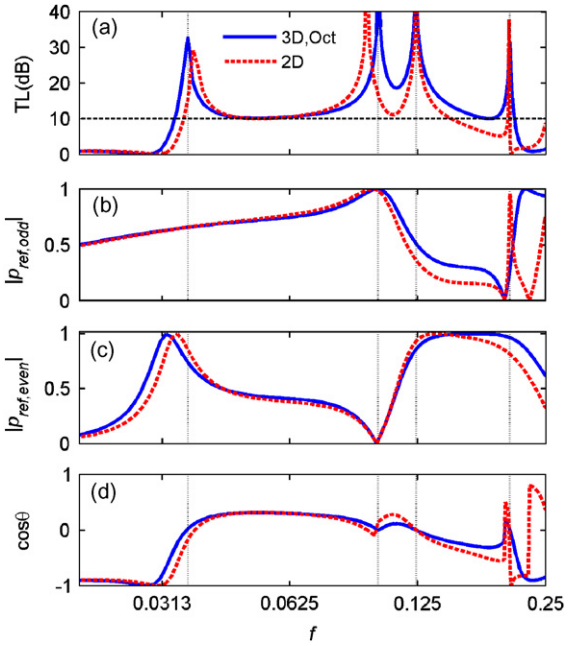

Fig. 10. Comparison of the optimal performance for the circular wave reflector (3D plate silencer III) with the 2D design of the same total cavity volume $\Lambda = 10$: (a) TL spectra. (b) Contribution by the odd axial modes towards the total sound wave reflection. (c) Contribution by the even axial modes towards the total sound wave reflection. (d) Odd–even interference index. The positions of the three spectral peaks are marked by vertical dotted lines.

maximum radial dimension. With the radial dimension reduced, the 3D configuration will fit the situations better where the installation space is limited.

3.2. Discussions

Owing to the 3D configuration, the sound field inside the duct also becomes complex for plate silencers I–IV. Fig. 9(a) shows a typical contour of the velocity potential inside the duct at the cross-section of $x = 0$ for $f = 0.05$ for plate silencer I. It is not surprising to see that the velocity potential distribution is no longer uniform along either y or z direction, and that the near pressure field inside the duct is really 3D. However, the plate vibrates in a rather 2D manner, as shown in Fig. 9(b). The approximate 2D response of the plate makes

it reasonable to investigate the modal vibration contribution to the total sound reflection in a 2D manner in the following vibroacoustics analysis.

The contributions to sound wave reflections made by different axial modes of the plate are studied. The velocity response of the plate vibration is decomposed into a series of *in vacuo* axial modes $\sin[j\pi(x/L+1/2)]$ with modal amplitude V_j, and the contribution of each single mode towards the total sound reflection p_r is analyzed. In doing so, the plate vibration velocity V is simply averaged over the width of the plate since the plate response is almost 2D, as already shown in Fig. 9(b). The contribution of each vibration mode, denoted as V_jR_j, towards the total sound reflection p_r is found by projecting the former to the latter. The result is called the modal reflection contribution γ_j. Here, R_j is the complex amplitude of the reflected sound by the induced vibration of the jth mode with unit amplitude. Expressions for R_j and γ_j can be found in Huang [1].

A comparative study is conducted on the vibroacoustic performance between the 3D (regular octagon duct with circular chamber) and 2D (rectangular duct with two opposite cavities) plate silencers, as shown in Fig. 10. The results for the 3D plate silencer are shown in solid lines and those of the 2D design are shown in dashed lines. The configurations for the two silencers are the same as those described in Section 3.1. Fig. 10(a) compares the TL spectra between the two types of silencers. The two designs are denoted by "3D, Oct" and "2D" in the figure legends, respectively. The frequency positions of the four peaks of the circular model are marked by vertical dotted lines for easy reference. The sound reflections from all odd modes are lumped as one spectral curve and compared in Fig. 10(b), and those from the even modes are compared in Fig. 10(c). The general patterns shown in Fig. 10(b) and (c) are similar for both the 3D and 2D designs. However, for the odd modes, the 3D design has better reflection at higher frequencies, which can be shown to be mainly from more constructive interference between the first and the third modes instead of from an enhanced first mode. For the even modes, the spectrum for the 3D design is stretched out towards lower and higher frequency regions relative to the 2D design. Apart from higher sound reflection, the improved cross-modal interference also accounts for the performance improvement of the 3D model from the 2D model in the relative high frequency, as shown in Fig. 10(d). The interference index is given by $\cos\theta$, in which θ is the phase angle between the reflected wave from the odd modes and that from the even modes. For frequencies between the third and fourth peaks, the odd–even interference for the 3D silencer is less destructive than that for the 2D silencer; hence, stronger total sound reflection is expected for the 3D design. As a summary, it is pointed out that the 3D design gives better plate response at higher axial modes than the simple 2D (two-cavity) design.

4. Hybrid silencer

A hybrid arrangement of plate silencer and traditional duct lining is proposed to combine the advantages of the two noise control methods. The full configuration of the hybrid silencer consists of two opposite reflection cavities and two dissipative chambers. Fig. 1 can be considered as a quarter model of the hybrid silencer with the bottom cavity working as the reflection cavity, and the back cavity as the dissipative chamber. The two reflection cavities are covered by plates with leading and trailing edges simply supported and other lateral edges free. For the two dissipative chambers, the sound absorbing material of the flow resistance R_{sam} is filled into them. All of the four cavities are of length $L = 5h$ and depth $h_c = h$, which is the optimal cavity shape for the two-cavity plate silencer with the volume of $Lh_c = 5h^2$ [2]. Such a configuration is similar to that of the four-cavity wave reflector except that only two out of the four cavities are used to reflect sound.

The performance of the hybrid silencer is optimized with respect to two controlling parameters: the bending stiffness B of the plates and the flow resistance R_{sam} of the sound absorbing material. Unlike in the case of wave reflector, the lower boundary limit f_1 is chosen as the cost function above which TL is higher than the criterion value, TL_{cr}. The optimal results found with the following configurations:

$$R_{\text{sam,opt}} = 1.4, \quad B_{\text{opt}} = 0.0627, \quad m = 1, \quad \text{TL}_{\text{cr}} = 10\,\text{dB} \tag{30}$$

are shown in Fig. 11. The frequency position of the lower limit f_1 is marked by a vertical line in the figure. As shown in Fig. 11(a), a wide stopband ranging from $f_1 = 0.0237$ to high frequency is obtained for the hybrid silencer. Fig. 11(b) and (c) shows the sound energy absorption coefficient α and the sound energy reflection coefficient β, respectively. An obvious peak can be observed just below frequency f_1 in Fig. 11(b), indicating that significant sound absorption occurs due to strong interaction between the plate vibration and the sound

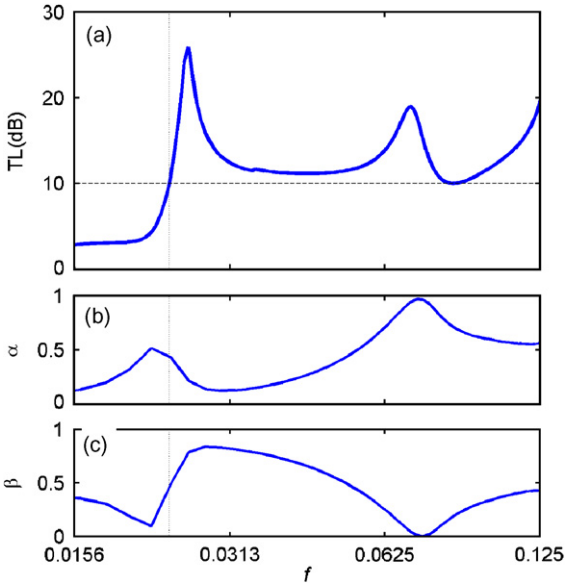

Fig. 11. Optimal performance of the hybrid silencer: (a) TL. (b) Absorption coefficient, α. (c) Reflection coefficient, β. The optimal bending stiffness $B_{\text{opt}} = 0.0627$ and optimal flow resistance $R_{\text{sam,opt}} = 1.4$ are obtained with the following parameters given: $L = 5$; $h_c = 1$, $m = 1$.

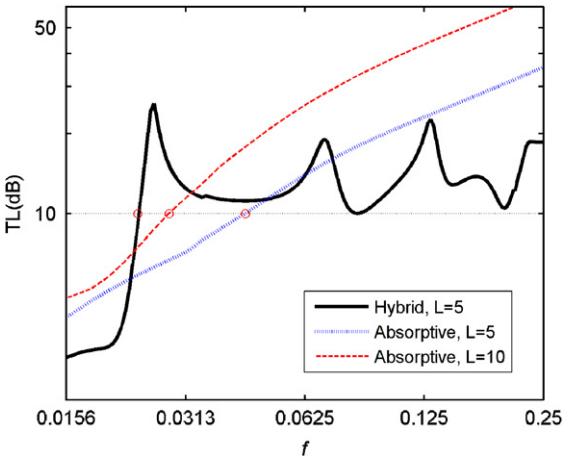

Fig. 12. TL comparison between the four-cavity hybrid silencer ($L = 5$, $B_{\text{opt}} = 0.0627$, $R_{\text{sam,opt}} = 1.4$) and a four-cavity absorptive chamber ($L = 5$, 10, $R_{\text{sam,opt}} = 1.4$). The cavity depth is $h_c = 1$ for the two designs.

absorbing material at that frequency. It is a desirable property that may improve the silencing performance of the hybrid silencer in low frequency. However, in general, sound wave reflection is still the main mechanism for noise reduction in the low-frequency region. Sound absorbing materials in the absorption cavities become effective only when the excitation frequency is high enough.

A comparative study is conducted between the hybrid silencer and pure sound absorption. In doing so, the plates covering the reflection chambers are removed and all the four cavities of the hybrid silencer are filled with sound absorbing materials. Such a device may be called a four-cavity absorptive chamber in the current context. The performance of the four-cavity absorptive chamber with two different configurations is calculated. In the first example, the absorption cavity is of length, $L = 5$, and depth $h_c = 1$, so that the total cavity volumes of the absorptive chamber and the hybrid silencer are equal. In the second example, the cavity length of the absorptive chamber is extended to $L = 10$ while the cavity depth remains $h_c = 1$. The flow

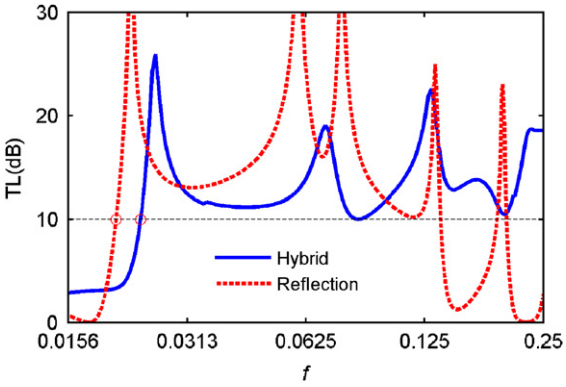

Fig. 13. TL comparison between a hybrid silencer and a four-cavity wave reflector of the same total cavity volume $\Lambda = 20$.

resistance R_{sam} of the sound absorbing material is optimized in the same way as in the case of the hybrid silencer. With a criterion value $\text{TL}_{\text{cr}} = 10\,\text{dB}$, the same optimal flow resistance $R_{\text{sam,opt}} = 1.4$ is found for the two configurations. Fig. 12 compares the TL spectra of the hybrid silencer (solid line) and the four-cavity absorptive chamber (dotted line, $L = 5$; dashed line, $L = 10$). Logarithmic scales are used on both axes. As shown in Fig. 12, the lower band limits for the three silencers, being marked by open circles for easy identification, are 0.0237, 0.0451, and 0.0284, respectively. The lower boundary of the hybrid silencer ($f_1 = 0.0237$) is almost half of the pure absorptive chamber of the same length $L = 5$ ($f_1 = 0.0451$), which demonstrating a significant improvement of the performance of the silencer in the low-frequency region. Doubling the length of the absorptive chamber can reduce its lower boundary to 0.0284 accordingly, but it is still higher than that of the hybrid silencer. Hence, compared with the pure absorptive chamber, one obvious advantage of the hybrid silencer is that it can achieve a good moderate bandwidth with a much reduced total length.

However, since the noise reduction in low frequency is mainly caused by sound reflection, a hybrid silencer cannot achieve better low-frequency performance than a pure wave reflector with the same cavity volume. In Fig. 13, the solid line shows the TL of the hybrid silencer investigated above, and the dashed line shows that for a four-cavity wave reflector with the following configuration:

$$L = 7.6, \quad Lh_c = 5, \quad B = 0.81, \quad m = 1. \tag{31}$$

The lower frequency limits of the four-cavity wave reflector and the hybrid silencer are $f_1 = 0.02$ and 0.0238, respectively, as marked by the two open circles. So, if the main concern is the low-frequency performance at the design stage, a wave reflector is preferred.

5. Concluding remarks

The acoustic benefit of using 3D configurations in a plate silencer design has been investigated numerically. The finite element simulation scheme is made out of a software package specializing in solving partial differential equations and multiphysics applications. The code is validated by known semi-analytical solutions. Finite element simulation shows that the 3D design expands the bandwidth in both lower and higher frequency regions relative to the corresponding 2D design. However, the advantage of adopting a 3D configuration mainly comes from the relatively higher frequency region, and its benefit in low frequency region is marginal. Of the four 3D silencers considered, the design of an octagon duct with circular chamber (type III) has the widest bandwidth, followed by the design of rectangular duct with circular chamber (type II), four-cavity wave reflector (type I), and the design of rectangular duct with rectangular chamber. Vibroacoustics analysis on the plates shows that the benefit of 3D design derives from better plate vibration response from axial modes of higher orders.

A hybrid silencer is proposed to combine the merits of the plate silencer and the traditional duct lining. Under the hybrid arrangement, the two-cavity plate silencer reflects the low-frequency sound waves, while the

dissipative chambers attenuate effectively the high-frequency sound energy. Compared with the pure absorption design, the hybrid silencer is able to achieve a good broadband noise reduction with much reduced total length. However, as far as the low-frequency performance is concerned, a four-cavity wave reflector outperforms the hybrid silencer with the same total cavity volume.

Acknowledgments

The first author thanks the Hong Kong Polytechnic University for the Ph.D. studentship. The main part of the reported work was carried out when the second author was employed at the Hong Kong Polytechnic University, with the support of a grant from the Research Grant Council of the Hong Kong SAR Government (5298/03E).

References

[1] L. Huang, Modal analysis of a drumlike silencer, *Journal of the Acoustical Society of America* 112 (2002) 2014–2025.
[2] L. Huang, Broadband sound reflection by plates covering side-branch cavities in a duct, *Journal of the Acoustical Society of America* 119 (2006) 2628–2638.
[3] Y.S. Choy, L. Huang, Experimental studies of a drumlike silencer, *Journal of the Acoustical Society of America* 112 (2002) 2026–2035.
[4] Y.S. Choy, L. Huang, Effect of flow on the drumlike silencer, *Journal of the Acoustical Society of America* 118 (2005) 3077–3085.
[5] S. Brown, Acoustic design of broadcasting studios, *Journal of Sound and Vibration* 1 (1964) 239–257.
[6] R.D. Ford, M.A. McCormick, Panel sound absorbers, *Journal of Sound and Vibration* 10 (1969) 411–423.
[7] K.V. Horoshenkov, K. Sakagami, A method to calculate the acoustic response of a thin, baffled, simply supported poroelastic plate, *Journal of the Acoustical Society of America* 110 (2001) 904–917.
[8] W. Frommhold, H.V. Fuchs, S. Sheng, Acoustic performance of membrane absorbers, *Journal of Sound and Vibration* 170 (1994) 621–636.
[9] M.L. Munjal, S. Krishnan, M.M. Reddy, Flow-acoustic performance of perforated element mufflers with application to design, *Noise Control Engineering Journal* 40 (1993) 159–167.
[10] C. Wang, J. Han, L. Huang, Optimization of a clamped plate silencer, *Journal of the Acoustical Society of America* 121 (2007) 949–960.
[11] F.P. Mechel, I.L. Vér, Sound-absorbing materials and sound absorbers, in: L.L. Beranek, I.L. Vér (Eds.), *Noise and Vibration Control Engineering, Principles and Applications*, Wiley, New York, 1992 (Chapter 8).
[12] L. Huang, Parametric studies of a drumlike silencer, *Journal of Sound and Vibration* 269 (2004) 467–488.